



Balanced bright and dark field illumination for remote visual testing to detect cracks on pressure vessel of nuclear reactors

Takeshi Shimano¹ · Keiichi Betsui¹

Received: 4 April 2021 / Accepted: 16 June 2021 / Published online: 28 June 2021
© The Optical Society of Japan 2021, corrected publication 2021

Abstract

Remote visual testing by video cameras is the standard process for inspecting the pressure vessel of nuclear reactors. The inspectors need to find stress corrosion cracking of around several tens of μm wide on a display monitor observed by remote wired cameras in the reactor pressure vessel filled with cooling water. The inside surface of the vessel structure has typically been blasted or grinded during its construction process for smoothing any excess weld metal, and as such, it might contain partly specular areas and partly rough areas. We found that the cracks on such surfaces are hardly distinguished from the boundary of these areas under normal scattered illumination, since the specular area reflects more of the light from the light source outside the path to the camera than the light scattered out by the rough area. To resolve this issue, we propose using two illumination light sources simultaneously, i.e., the bright field illumination and the dark field illumination, to balance the contrast to cracks from both areas. The results of experiments in a simplified condition showed that there was an improvement in the visibility of the cracks using this method.

Keywords Remote visual testing · Crack inspection · Bright field illumination · Dark field illumination

1 Introduction

After the Great East Japan Earthquake in 2011, the safety of nuclear power plant has been increasingly scrutinized. To maintain the safety, periodic inspections and special inspections have been strictly performed from before the disaster for all nuclear power plants in Japan. During past inspections, stress corrosion cracks on structure bodies in nuclear reactors have been reported, which is concerning, because these are at risk to rupture as the cracks extend. Therefore, visual testing (VT) is required to be performed in all nuclear power plants to find any cracking as early as possible. [1]

With VT, the visual inspection can be done remotely using cameras to examine the surface of the structure bodies in cases where the inspectors cannot look directly with their own eyes, as is the case when inspecting the inside of the pressure vessel of nuclear reactors filled with cooling water.

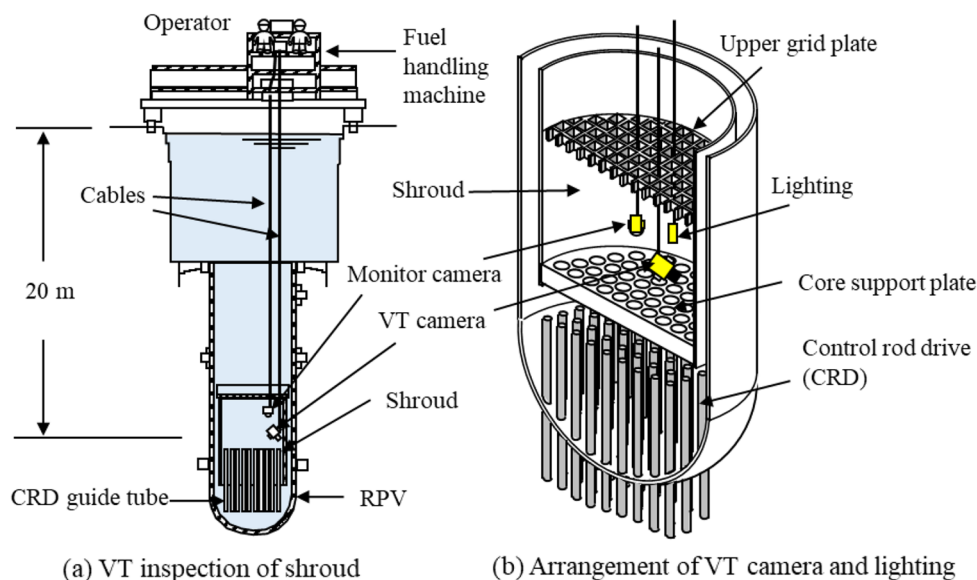
The inspectors watch the monitored live video of images of the surface of the structure body in the pressure vessel captured by a wired camera with appropriate illumination to the surface. If any defects are discovered during VT, further ultra-sonic testing (UT) or eddy current testing (ECT) is carried out.

Figure 1 shows a schematic view of VT inspection. One of the main inspection targets is the surface of the shroud in the reactor pressure vessel (RPV), which is filled with cooling water. The shroud is generally made of stainless steel in natural metallic gray color whose surface has not-shiny texture in general and partly shiny due to repairs or mechanical cleaning [1]. During the inspection, the fuel rods are removed, but the upper grid plate remains. Therefore, the inspection operation needs to be performed through holes sized about 300 mm square on the upper grid plate. Operators control the positions of the camera and illumination lighting and inspectors then judge the defects on the monitored video. Since the width of crack opening tends to be about several tens of μm , the field size of the monitored video should be about 20–30 cm square on the shroud. Therefore, the VT camera view needs to be scanned by moving the position of the camera, which takes a long time for both the operators and the inspectors. While the monitor

✉ Takeshi Shimano
takeshi.shimano.rb@hitachi.com

¹ Center for Technology Innovation–Electronics and Instrumentation, Hitachi, Ltd., Research and Development Group, 1-280 Higashi-Koigakubo, Kokubunji, Tokyo 185-8601, Japan

Fig. 1 Schematic view of VT inspection



camera in the figure is used to record the viewpoint of the VT camera in wider view, simultaneously.

There have been many research activities related to detection of defects for various applications. Kubiak et al. [2] proposed infrared light beam scanning on the inspection surface to detect scattered light by the defects. Pernick et al. [3] [4] proposed laser beam scanning with Fourier analysis to find 0.5 μm -wide cracks. Tippur et al. [5] simultaneously measured deformations and cracks by a combination of Moiré topography and laser speckle measurement. Zhang et al. [6] analyzed scattered light by cracks on glass depending on their structure using the finite difference time domain (FDTD) method. However, all the above works assumed a basically smooth inspection surface for the target, which is not always possible with the RPV shroud because of its variation of roughness.

Choi et al. [7] proposed image processing using a Gabor filter to detect seam cracks in steel plates. Lin et al. [8] reported a micro-crack detection system on a Si wafer in a dicing process using near-infrared light. Z. Dong et al. [9] proposed predicting damage trends and finding a strategy for grinding the lens-cup wheel. J. Dong [10] proposed a line-scanning laser scattering system for fast defect inspection. Yang et al. [11] reported defect detection on the surface of large steel roller surfaces using a machine vision technique called the active contour model for images detected by a line-scan camera. This method is essentially based on image processing to segment the image in accordance with texture on the surface. While these defect detection technologies work for non-smooth surfaces, they differ from our work in that they are not directly focused on lighting technology for VT.

In an example for lightning technology for defect detection, a technology white paper for machine vision lighting

[12] has been provided by Microscan Systems Inc. on their website. They summarized tips for choosing the right lighting for machine vision application and suggest using non-diffused light as dark field lighting for detecting cracks on a transparent glass bottle. However, they do not examine crack detection on partly shiny or partly rough surface areas, which we assume for the RPV shroud surface.

There are several patents and patent applications for surface inspection methods that simultaneously using bright and dark field illumination [13] [14] [15]. Nakano et al. [13] proposed an inspection system for both specular and scattering surfaces by switching between bright and dark field illumination. Matthieu et al. [14] proposed an inspection system that can emphasize the specular region from the non-specular region on a printed circuit substrate. They alternatively illuminate the substrate by bright and dark field light and capture the images of the surface independently. By having the light intensity obtain the same brightness in the non-specular region, the specular region is emphasized in the digital subtraction image of captured images. However, they did not examine crack inspection. Adachi et al. [15] proposed a surface inspection system that emphasizes cracks by the image processing of bright and dark field images. Their concept is quite similar to our own but differs in that they take bright and dark field images independently and create an emphasized crack image from these two images.

In this paper, we focus on illumination technology to maximize the visibility of cracks through the conventional VT process and to minimize the possibility of passing over the defects of cracks without flagging them. The inside surface of the vessel has typically been blasted or grinded during its construction and maintenance process for smoothing any excess weld metal. As such, it might contain partly specular areas and partly rough areas. We

found that the narrow cracks on such surfaces are hardly distinguished from the boundary of these areas under normal scattered illumination, which basically corresponds to dark field illumination. This is because the specular area removes more of the light from the light source out of the path to the camera than the light scattered out by the rough area. We propose using two illumination light sources simultaneously, i.e., bright field illumination and dark field illumination, to balance the contrast to cracks from both areas. The results of experiments in a simplified condition showed that there was an improvement in the visibility of the cracks using this method.

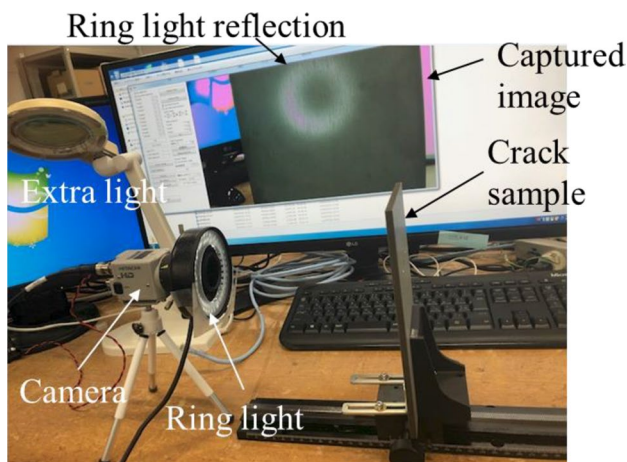


Fig. 2 First experimental setup to observe crack on test piece plate

2 Experiments

2.1 Basic experimental condition

Figure 2 shows the first experimental setup and Table 1 lists the specifications. The surface of the crack sample plate is observed by a video camera and the monitored image is displayed on the monitor screen of an LCD display. The surface is illuminated by a ring light attached to the camera and other lights such as a fluorescent extra light or ceiling lights in the laboratory. The crack sample is made of stainless-steel imitating standard shroud surface according to the experiences in Hitachi GE Nuclear Energy Ltd. during nuclear plant operation and maintenance business and to the knowledge as the results of collaboration with electric power companies for VT technology development. The crack on the test piece plate is generated by a stress induced by processing a zigzag groove several millimeters in width and of a few millimeters in depth on the back side of the plate by a mechanical milling machine. The crack opening dimension, namely, the width of the crack is about $8\ \mu\text{m}$. Object distance is determined, so that the crack can be recognized on the monitor screen. Since the focal length of the lens is 8 mm, the magnification is about 30 when the object distance is 250 mm. Therefore, the geometrical image width of the crack becomes $0.27\ \mu\text{m}$ on the image sensor, which is much smaller than the pixel pitch of $2.8\ \mu\text{m}$ or the diffraction limit spot size of $2.2\ \mu\text{m}$ for F number 1.95. This does not mean that the crack is invisible on the screen; rather, it is visible in the contrast factor of about $0.27/\max(2.8, 2.2) = 0.096$, as the crack is normally isolated in our application. During the experiment, we assume that we can recognize the crack in the condition that the contrast factor is larger than about 0.07. To obtain a larger field view to reduce scan times, a

Table 1 Specifications of experimental setup

Components	Items	Specifications
Crack sample	Size	200 mm × 120 mm × 5.8 mm
	Material	Stainless steel (SUS304)
	Surface property	Acid pickling surface (Satin finished)
	Crack opening dimension	1.7–7.8 μm
	Crack shape	Zigzag
Camera	Product model	Hitachi Kokusai Electric, KP-HD20A
	CMOS sensor	1/3-inch, 1944 × 1092 pixels
	Signal output	HD-SDI, YUV4:2:2, 10bit
Lens	Product model	Tamron, M13VM288IR (Vari-focal)
	Focal length	2.8–8 mm (Experiment: 8 mm)
	F number	1.2 (Wide)–1.95 (Tele)
	Object distance	25 cm
Ring light	Product model	Armssystem Ltd., LED-R72, AC100V, 7.2 W
Extra light	Product model	Elaice Ltd., Lumiloupe, AC100V, 12 W

larger magnification (namely a smaller focal length) would be better. However, a magnification that is too large fails in terms of too small a contrast and invisible cracks. On the other hand, a larger crack image size on the image sensor to increase the image contrast results in a smaller field view and increases the scan times. Therefore, we opted for the specification in Table 1 to obtain the smallest image at the minimum contrast for VT.

2.2 Surface property of the crack sample plate

Since we assumed that the surface would have a dominantly diffusing property for incident illumination light due to its rough visual appearance at first, we chose the ring light for main illumination, as shown in Fig. 2. However, we noticed that the direct specular reflection of the ring light was rather dominant in the captured camera image, as can be seen in the figure. Therefore, we investigated the optical surface property using the Mini-Diff scattering property measurement tool [16]. Figure 3 shows the measurement results of the bidirectional scattering distribution function (BSDF) of the crack sample plate for incident light angles of (a) 0 deg, (b) 20 deg, (c) 40 deg, and (d) 60 deg. The direct reflection peak was dominant at the corresponding reflection angle in

each incident angle case with scattering light around it in the range of a 20-degree angle width. This explains the appearance of the ring light image in Fig. 2. While this might not be a typical case of the surface property of the RPV shroud, we presume that we should be ready for surface variations between the specular and scattering surfaces. In that sense, we tried to improve the visibility in this sample as an intermediate case between specular and scattering.

2.3 Oblique observation condition

To avoid specular ring light reflection, we next examined the oblique illumination condition, as shown in Fig. 4. The optical axis was initially tilted to the inspection surface normal, and then, we tried to find the best visibility condition by switching the ring light on/off, blocking/not blocking the ceiling light, and putting/not putting white diffuser (note paper, in fact) beside the sample. The optimum case was when the ring light and ceiling light were both on and white diffuser was included.

Figure 5 shows the observed crack images for (a) optimum condition, (b) ring light off condition, and (c) white diffuser removed condition. The pictures on the left are in wide ranges, and those on the right are magnified pictures

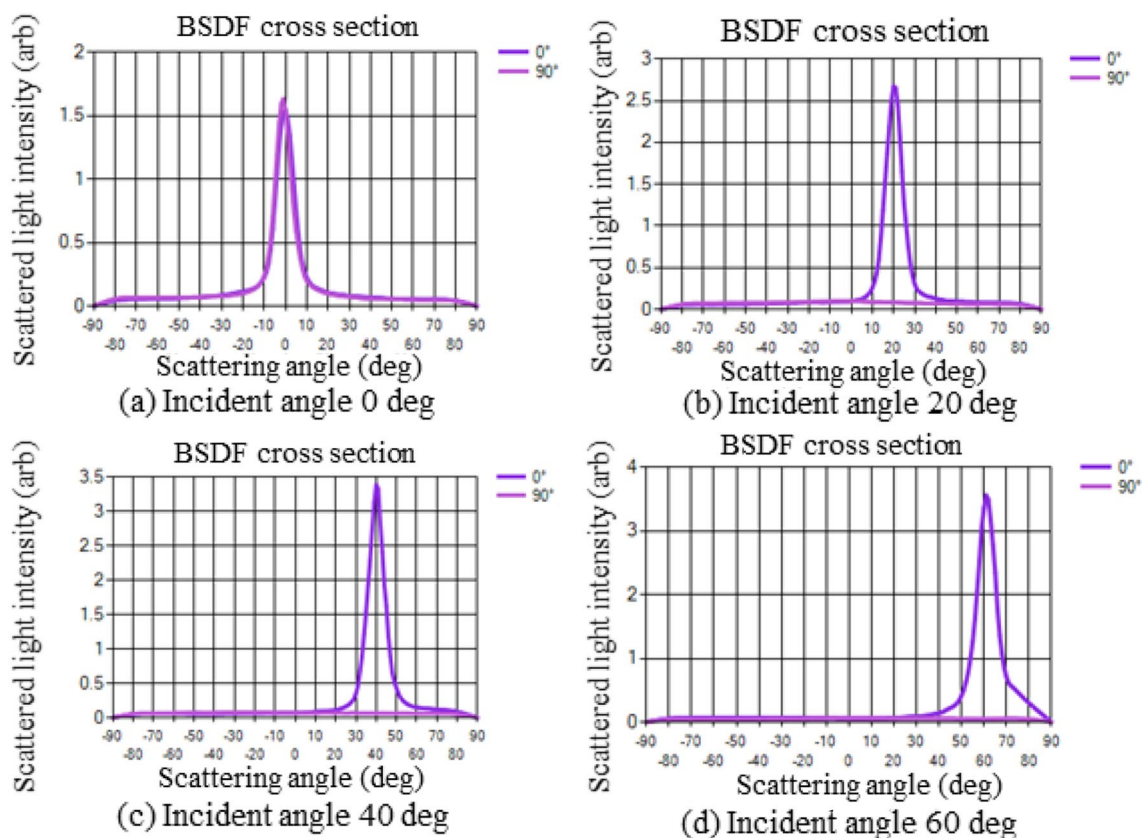


Fig. 3 Measurement results of bidirectional scattering distribution function of crack sample plate

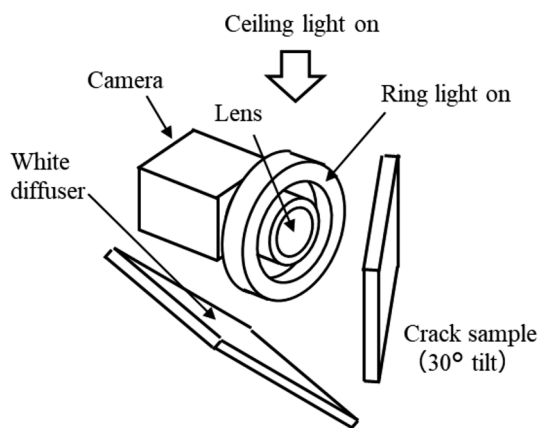


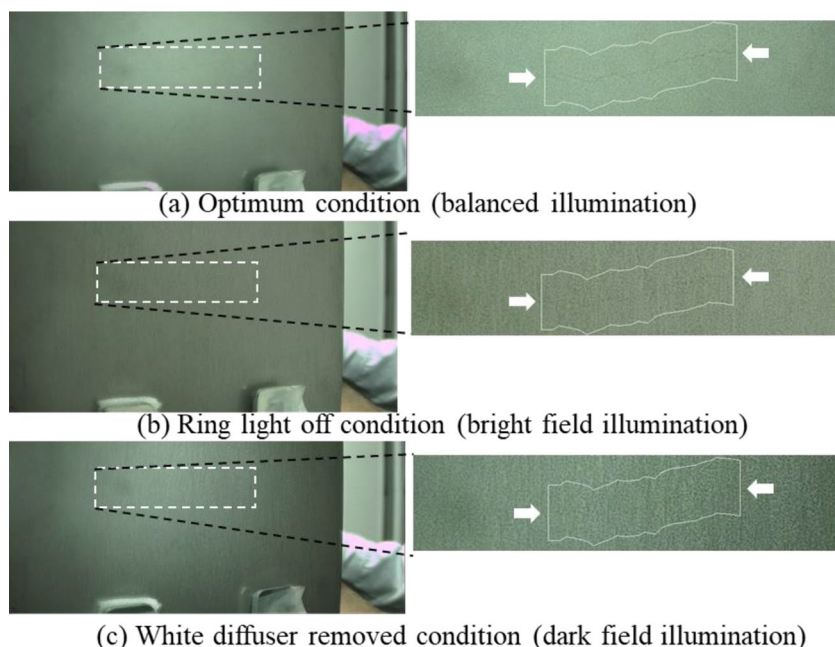
Fig. 4 Oblique optimum observation condition

of the broken white line squared area in the corresponding pictures on the left. The white enclosing lines in the magnified pictures denote existence of the horizontal cracks inside. The upper and lower zigzag lines of an enclosing line denote the locus of the crack apart 50 pixels from the crack center toward both upper and lower sides. The shape and pixel position of the crack are measured by plotting mouse pointers on an image display using a general image analysis software. Bold arrows in the right-side pictures also represent the existence of crack just in their directions. The term “optimum” in this case means the optimum visibility of the crack image in the display by subjective impression of the authors’ view. Visibilities of the crack images in conditions (b) and (c) were lower than that in optimum condition (a) due to surrounding roughness

textures in them. On the other hand, the contrast of these roughness textures seems to have been suppressed in the optimum condition. Please note that the visibility in this case is somewhat different from that is to be used for optical interference fringe in the interferometers. The visibility in the interferometer is usually defined as the contrast ratio of periodic intensity variation amplitude of the fringe to the maximum intensity. However, the visibility in this paper is related not only to the contrast of the crack image itself, but also to surrounding visual noise caused by the boundaries between mirror areas and roughness areas. Since we think that our proposing method is effective for reducing the noise, we discuss it quantitatively in the chapter 2.5.

Anyway, we measured the contrast of the crack image in Fig. 5. Although, the pixel brightness included noise due to surface roughness and the crack opening was not constant toward crack direction, we estimated the average profile by integrating the brightness profile toward the crack and by centering the perpendicular position to the crack during the integration. Figure 6 shows the averaged crack brightness profiles. The pixel intensities in 8 bits (maximum 255) toward 344 columns in horizontal pixel direction were averaged in each row with centering the crack position row to obtain averaged profile in 100 pixels toward perpendicular direction crossing the crack. The contrast values in the figures were calculated by dividing the depth of the valley of the crack by the average intensity except the crack area. The contrast value was the largest (0.048) in the dark field illumination condition; however, the noise relative to the valley depth was obviously larger than balanced illumination condition.

Fig. 5 Crack observation images for a optimum, b ring light off, and c white diffuser removed conditions



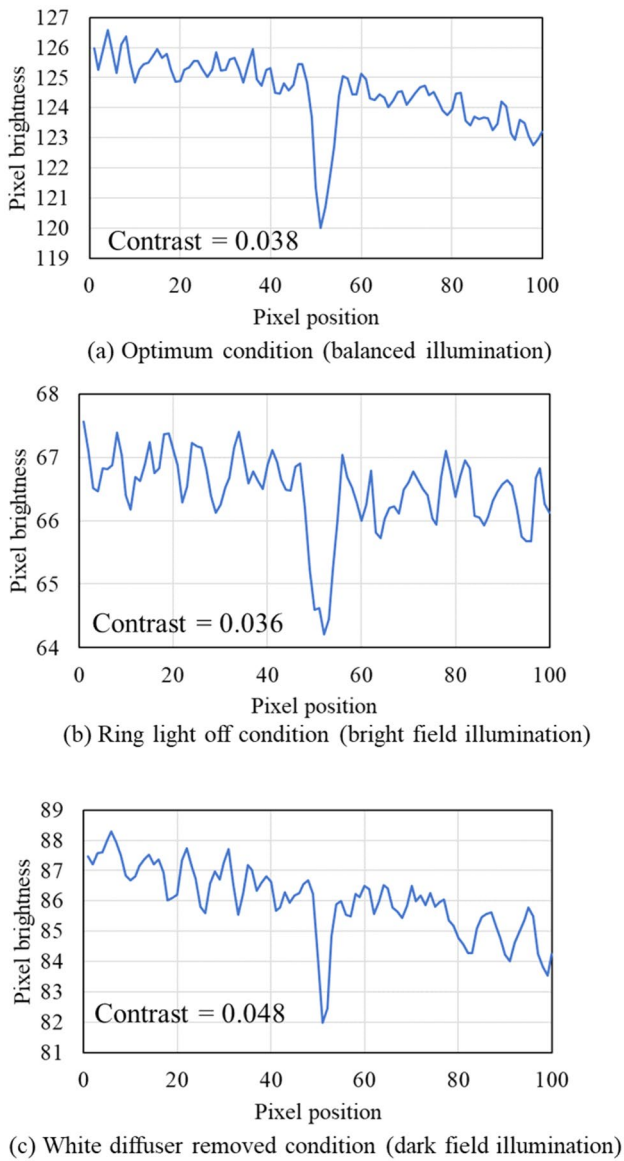
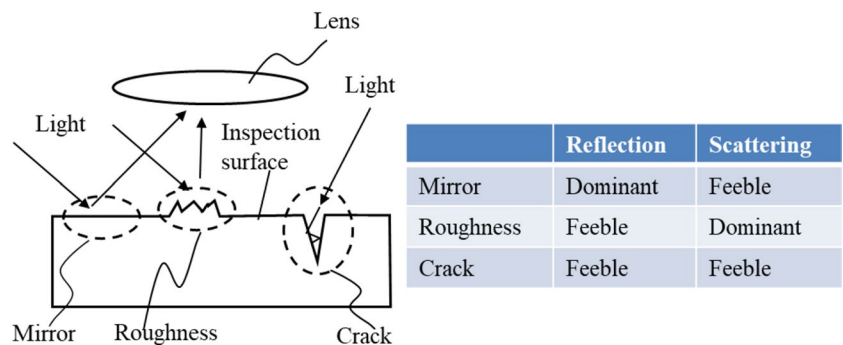


Fig. 6 Averaged image intensity profile crossing the crack in Fig. 5

Fig. 7 Presumption of light interaction characteristics between on inspection surface depending on surface features



Therefore, subjective visibility in this case was supposed to be mainly depending on signal-to-noise ratio, but not on the contrast ratio.

2.4 Mechanism underlying visibility improvement

We next investigated the mechanism underlying the visibility improvement in the optimum illumination condition in Fig. 5. As we have seen in Fig. 2 and Fig. 3, the surface of the crack sample plate has both specular and scattering properties. We presume these features as shown in Fig. 7. The surface had both mirror areas and roughness areas separately on the inspection surface with the crack area. In the mirror area, incident light is dominantly reflected, and scattering light is feeble. On the other hand, in the roughness area, incident light is dominantly scattered, and reflection is feeble. In the crack area, since the width of the opening must be much smaller than the depth, both side walls are approximately parallel. Therefore, incident light to the crack may be repeatedly reflected between both walls and comes out neither as reflection nor scattering.

Since the surface normal of the mirror area can be assumed to be rigid, the incident illumination light angle would be limited, so that the reflected light can be captured by the lens. When the light at that angle irradiates the roughness area, scattered light dominantly goes to various angles from the reflected light. Therefore, that scattered light could not be captured by the lens. Other incident illumination light in different incident angles from that of the reflected and captured light could not be captured as reflected light but only as scattered light in the roughness area. Consequently, illumination lights for reflected light and for scattered light could be distinguished by the incident angle.

Figure 8 represents the appearance of the captured image depending on the difference of the ratio between reflected light and scattered light. The upper box shows the assumption of the surface structure, which contains the mirror area, the roughness area, and the crack area. The lower three boxes show image appearances due to a difference of the ratio between reflection and scattering. When the reflection is dominant, the mirror area is bright and both roughness

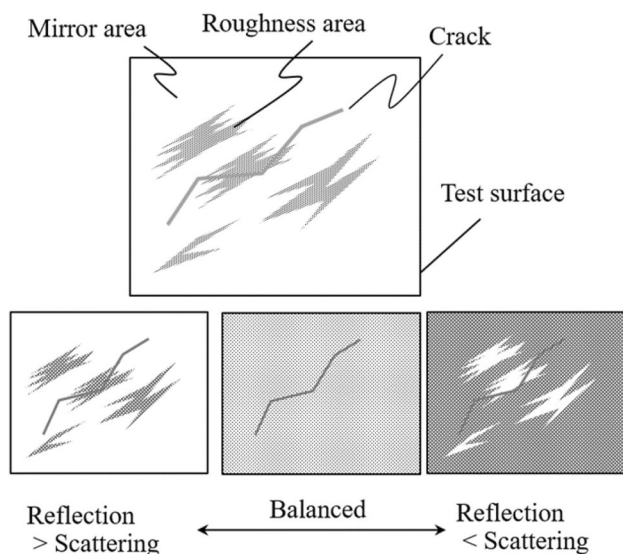


Fig. 8 Crack visibility dependence due to illumination conditions

and crack are dark. When the scattering is dominant, roughness area is bright and both mirror and crack area are dark. In both cases, the crack is hardly distinguished from mirror area or roughness area. On the other hand, in the intermediate condition of these two cases (namely, in the balanced condition), brightness of the mirror area and the roughness area could be the same as each other, which is still brighter than the crack area. Consequently, the boundary between mirror area and the roughness area could disappear and the contrast of the crack area could be seen to be emphasized.

In view of this consideration, the optimum condition in Fig. 5 can be understood as follows. The scattered light by the white diffuser is reflected by the surface of the crack sample plate and captured by the lens as reflected light on

the inspection surface. The light from the ring illumination is scattered by the surface of the crack sample plate and captured by the lens as scattered light on the inspection surface. Therefore, Fig. 5(b) corresponds to the reflection-only case, and Fig. 5(c) corresponds to the scattering-only case, and Fig. 5(a) is the balanced condition.

With reference to preceding literature [12] [13] [14] [15], we can conclude that reflection illumination corresponds to the bright field illumination and scattering illumination corresponds to the dark field illumination.

2.5 Balanced illumination configuration in vertical observation condition

We have described balanced illumination to emphasize the crack for an oblique observation condition. However, when the optical axis is tilted to the surface normal of the inspection surface, the focused area might be limited because of the limited focal depth of the imaging optics. We therefore tried to make a balanced illumination in the vertical observation condition. As can be seen in Fig. 2, the ring light image was localized in a small area of the displayed image. Therefore, we tried to magnify the ring light provisionally using a large paper plate with an observation hole at the center, as shown in Fig. 9. Other specifications of the setups are the same, as shown in Table 1. The camera observes the inspection surface through the hole in this case. Figure 9(a) corresponds to the balanced illumination condition by the large paper plate as the bright field illumination and the fluorescent extra light as the dark field illumination. In this case, the light from the ceiling light of the laboratory is shaded by thick papers. Therefore, the extra light was simultaneously used as a light source for the large paper plate. Figure 9(b) corresponds to the conventional illumination condition in which the normal ring light comes from behind the large

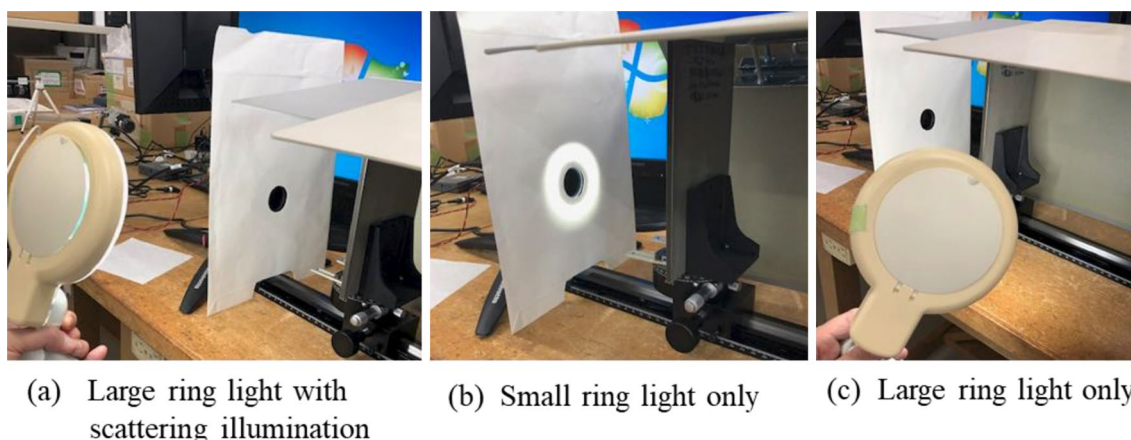


Fig. 9 Experimental setups for vertical observation of **a** balanced illumination condition by large ring light with scattering illumination, **b** small ring light only for reference, and **c** large ring light only for reference

paper plate without the extra light. Figure 9(c) corresponds to the bright-field-illumination-only case by illuminating the large paper plate by the extra light from behind the crack sample plate, so that it does not illuminate the crack directly.

Captured images of the setup in Fig. 9 are shown in Fig. 10 with roughness appearance as dispersion of pixel brightness of the surrounding area. The images in Fig. 10a–c were captured by the setups, as shown in Fig. 9 (a), (b), and (c), respectively. Even in the balanced illumination condition of Fig. 10 (a), the shadow of the center hole remained; however, its contrast was more softened than in the conventional condition (b). The white broken-line box in each image represents the crack area. The histogram in each image is the number of pixels in the yellow solid line box at each brightness from 0 to 255 on the horizontal axis. Since the local average of the brightness gradually changed in each image, we chose a smaller sampling

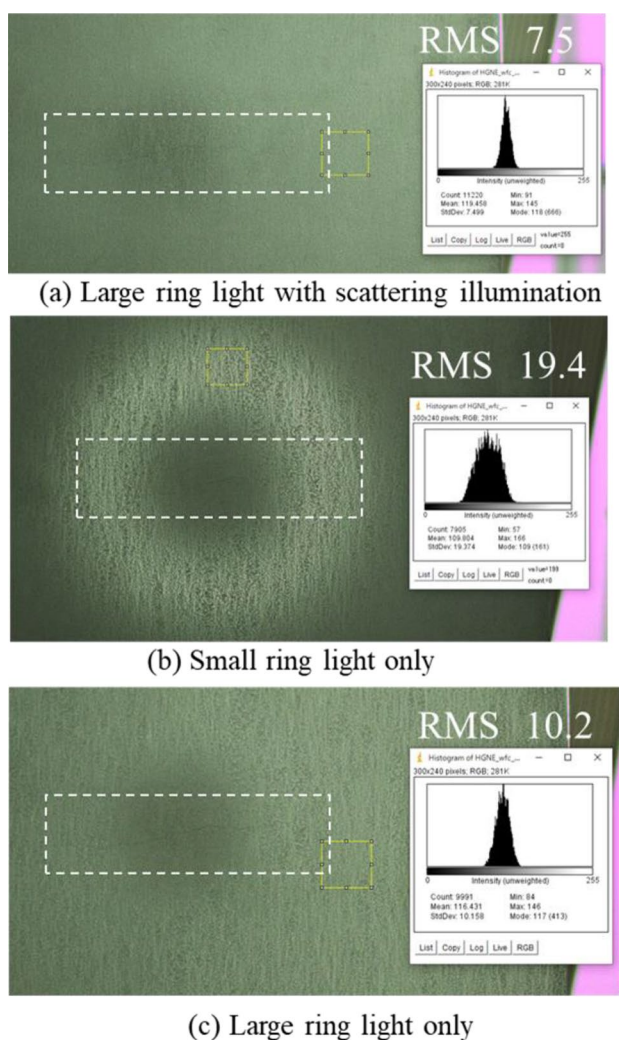


Fig. 10 Images captured under **a** balanced illumination condition, **b** conventional illumination condition, and **c** bright field illumination with pixel brightness dispersion

area for the histogram. The results show that the balanced illumination decreased the root-mean-square value of the brightness variance due to surface roughness from 19.4 to 7.5. On the other hand, the crack visibility of Fig. 10 (a) was better than (b), but not so different from (c); in fact, it might be rather worse. That is because the crack was almost in the shadow area of the hole in the large white paper plate. In that area, the bright field illumination became weak due to the blur of the hole, so it seemed to be almost the dark field illumination area. Accordingly, in Fig. 10 (c), the shadow area became a weak bright field illumination area, but probably the area was illuminated by scattered light from some other surrounding object. Thus, it might become rather closer to the balanced illumination condition than (a).

To investigate the improvement of crack visibility, the crack area images in Fig. 10 are magnified in Fig. 11. The center area of each images is the hole shadow area. The left side of the images is the appropriate illuminated area. When we compare the visibility of the crack in the left-side area between (a) and (c), it was obviously better in (a). This result demonstrates that the proposed balanced illumination improved the visibility of the crack, even in the vertical observation configuration.

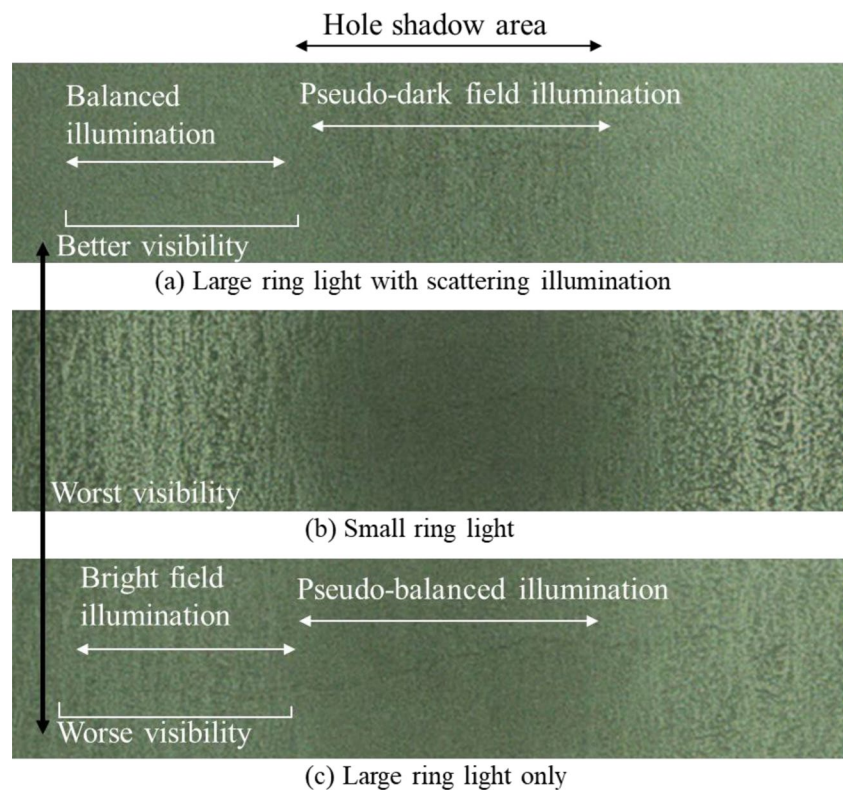
3 Future work

Since the work reported in this paper is a preliminary study for VT to detect cracks on RPV, we would like to clarify what we should do hereafter in this section. Followings are the remaining tasks.

- (1) Experiment using a surface emitting illumination for bright field illumination.
- (2) Experiment under water.
- (3) Oblique observation condition with some expanded depth of field (EDOF) technology [17] [18].
- (4) Radiation resistance of the system.
- (5) Size optimization of the bright field illumination for actual VT in RPV.

Regarding task (1), it is necessary to confirm active balancing between bright and dark field illumination. In this paper, we employed a white diffuser with uncontrollable light irradiating it for bright field illumination. Therefore, we have not confirmed real active balancing. For the uniformity of the bright field illumination, surface emitting device like water-proof LED plate would be preferable, simultaneously for task (2). With regard to task (3), EDOF technology would be effective in oblique illumination configuration to avoid center shadow hole of vertical illumination configuration. We also should prepare for task (4) and (5) to use in actual RPV.

Fig. 11 Magnified crack images of vertical observation configuration



4 Conclusion

In this paper, we proposed a balanced bright and dark field illumination for remote visual testing to detect cracks on the shroud of a reactor pressure vessel. To investigate the principle, we examined both oblique and vertical observation configurations in the relationship between optical axis and surface normal of the inspection surface. In both configurations, we found an improvement in the visibility of the crack. The mechanism underlying the improvement was clarified in a simplified model. In the vertical observation condition, we measured the brightness variation of the pixels due to surface roughness in the captured image and found that it could be successfully suppressed from 19.4 to 7.5 in the experiment. We will enhance the research considering more actual usage in RPV.

Acknowledgements We thank Dr. Narishige and Mr. Oshima of Hitachi Ltd. for providing the information in Fig. 1 and about the inspection process of the pressure vessel of nuclear reactors. They also provided us the crack sample which they made with Hitachi-GE Nuclear Energy, Ltd. We also thank Dr. Nagashima, and Mr. Naganuma of Hitachi-GE Nuclear Energy, Ltd. and Mr. Miki and Mr. Hosoya of Hitachi Ltd., for the valuable discussion.

Declarations

Conflict of interest On behalf of all authors, the corresponding author states that there is no conflict of interest.

References

1. Electric Power Research Institute Technical Report, Remote Visual Testing Round-Robin Study. (2016). <https://www.epri.com/research/products/3002007793>. Accessed 18 May 2021
2. Kubiak, E.J.: Infrared detection of fatigue cracks and other near-surface defects. *Appl Opt* **7**(9), 1743–1747 (1968)
3. Pernick, B. J., et. al.: Optical method for fatigue crack detection. *Appl Opt* **19**(18), 3224–3229 (1980)
4. Pernick, B.J., et al.: Fatigue crack detection on rough surfaces by optical Fourier analysis. *Appl opt* **24**(12), 1764–1769 (1985)
5. Tippur, H.V., et al.: Analysis of combined moire and laser speckle grating methods. *Appl Opt* **30**(19), 2748–2756 (1991)
6. Zhang, L., et al.: Systematic investigation on light intensification by typical subsurface cracks on optical glass surfaces. *Appl Opt* **52**(5), 980–989 (2013)
7. Choi, D.-C., et al.: Algorithm for detecting seam cracks in steel plates using a Gabor filter combination method. *Appl Opt* **53**(22), 4865–4872 (2014)
8. Lin, S.-F., et al.: Near-infrared imaging system for nondestructive inspection of micro-crack in wafer through dicing tape. *Appl Opt* **54**(28), E123–E128 (2015)
9. Dong, Z., et al.: Developing a trend prediction model of subsurface damage for fixed-abrasive grinding of optics by cup wheels. *Appl Opt* **55**(32), 9305–9313 (2016)
10. Dong, J.: Line-scanning laser scattering system for fast defect inspection of a large aperture surface. *Appl Opt* **56**(25), 7089–7098 (2017)
11. Yang, J., et al.: Development of an optical defect inspection algorithm based on an active contour model for large steel roller surfaces. *Appl Opt* **57**(10), 2490–2498 (2018)
12. Microscan Systems Inc., “Eight Tips for Optimal Machine Vision Lighting”. www.microscan.com (2011). Accessed 15 Sept 2020

13. Nakano, K., et al.: Illumination device, recognizing device with the illumination device, and part mounting device. US Patent, US 7,502,170 B2, (2009). Accessed 10 Mar 2009
14. Mattheiu, R., et al.: Surface inspection system and surface inspection method. Patent Application, WIPO PCT 2017/207116 A1 (2017)
15. Adachi, H., et al.: Image recognition apparatus. Japanese Patent Application, 2016–205876 (in Japanese) (2016)
16. Promiss Electro-Optics bv. <https://www.peo-electro-optics.com/en/product/mini-diff-westboro-photonics/>. Accessed 25 June 2021
17. Dowski, E.R., et al.: Expanded depth of field through wave-front coding. *Appl. Opt.* **34**(11), 1859–1866 (1995)
18. Ohta, M., et al.: Rotationally symmetric wavefront coding for extended depth of focus with annular phase mask. *Jpn J Appl Phys.* **54**, 09ME03 (2015)

Publisher's Note Springer Nature remains neutral with regard to jurisdictional claims in published maps and institutional affiliations.